Gamow-Teller strength in ^{23}Na(n,p) and a comparison to ^{23}Na(μ^-,ν)

B. Siebels,[1] T. P. Gorringe,[1] W. P. Alford,[2] J. Bauer,[1] J. Evans,[1] S. El-Kateb,[5] K. P. Jackson,[3] A. Trudel,[4] and S. Yen[3]
[1]*Department of Physics and Astronomy, University of Kentucky, Lexington, Kentucky 40506*
[2]*Department of Physics, University of Western Ontario, London, Ontario, Canada N6A 3K7*
[3]*TRIUMF, 4004 Wesbrook Mall, Vancouver, Canada V6T 2A3*
[4]*Department of Physics, Simon Fraser University, Vancouver, British Columbia, Canada V5A 1S6*
[5]*King Fahd University of Petroleum and Minerals, Dhahram, Saudi Arabia*
(Received 6 April 1995)

We report measurements of the ^{23}Na(n,p) differential cross section at an incident energy of 198 MeV and angles from 0° to 24° using the TRIUMF Charge Exchange Facility. From these data we determine Gamow-Teller (GT) transition probabilities to low lying $1/2^+$, $3/2^+$, and $5/2^+$ ^{23}Ne states and the GT$^+$ strength distribution up to 25 MeV excitation energy. The values of B_{GT}^+ to discrete states, and the GT$^+$ strength below 10 MeV, are found to be in reasonable agreement with a full $1s$-$0d$ shell model calculation with a normalization factor of about 0.74. The GT$^+$ strength above 10 MeV suggests the removal of strength from lower to higher excitation energies. We also compare the ^{23}Na(n,p) data with ^{23}Na(μ^-,ν) data and find agreement between the values of B_{GT}^+ to discrete levels extracted from the (n,p) and (μ^-,ν) reactions. The general consistency of the (n,p) and (μ^-,ν) data, and the full $1s$-$0d$ shell model calculation, give confidence in a recent extraction of the weak pseudoscalar coupling from μ^- capture on ^{23}Na. Finally, using both β^--decay and μ^- capture data, we obtain unit cross sections from the ^{23}Na(n,p) measurement.

PACS number(s): 25.40.Kr, 23.40.−s, 24.30.Cz, 27.30.+t

I. INTRODUCTION

A major discovery in nuclear physics was that the (p,n) and (n,p) charge exchange reactions, at medium energies and forward angles, provide an unambiguous signal of spin-isospin (Gamow-Teller) transitions in nuclei [1,2]. The discovery has led to the use of these reactions to explore Gamow-Teller (GT) strength in nuclei from the determination of GT matrix elements that govern stellar collapse [3–5], double β-decay [6], and neutrino detection [7], to the investigation of GT quenching.

The $(p,n)/(n,p)$ reaction can also be a valuable tool in the extraction of the weak pseudoscalar coupling from measurements of μ^- capture on nuclei. The nucleon's weak pseudoscalar coupling g_p is induced by the effects of its strong interaction on its weak interaction. In the partially conserved axial current (PCAC) hypothesis [8] g_p is due to single-pion exchange between the leptonic and nucleonic currents in semileptonic weak processes. It predicts $g_p/g_a = 6.7 \pm 0.2$ [9] in agreement with the free nucleon experimental value $g_p/g_a = 6.9 \pm 1.9$ [10]. In a nucleus, however, g_p may be different—indeed measurements of radiative μ^- capture (RMC) on nuclei [11,12] have suggested the intriguing possibility of a large g_p enhancement in light nuclei and a large g_p quenching in heavy nuclei. These suggestions are, however, contentious and a recent measurement of the hyperfine effect for several GT transitions in ordinary μ^- capture (OMC) on ^{23}Na yields $g_p/g_a = 7.6 \pm {}^{2.1}_{2.5}$ [13], consistent with the free nucleon value of g_p. An important test of the extraction of g_p/g_a from the $\mu^-{}^{23}$Na data is a determination of the ^{23}Na $\rightarrow$ ^{23}Ne GT matrix elements. The GT matrix elements are the dominant matrix elements in the measured $\mu^-{}^{23}$Na transitions and their determination is therefore the best test of the nuclear model used to extract g_p/g_a from the data. Agreement between the measured and calculated ^{23}Na $\rightarrow$ ^{23}Ne GT matrix elements would build confidence in the value of g_p/g_a extracted from the $\mu^-{}^{23}$Na data. Since these GT transitions are inaccessible to β-decay, the (n,p) reaction on ^{23}Na, at medium energies and forward angles, is the natural choice for this determination.

The $1s$-$0d$ shell model of nuclei between ^{16}O and ^{40}Ca represents the most successful application of the shell model in nuclear physics. A benchmark test of the the $1s$-$0d$ shell model has been the comparison of measured and calculated GT strength distributions in the $(p,n)/(n,p)$ reactions on a number of $N=Z$ $1s$-$0d$ nuclei [14]. These comparisons show general agreement between measurement and calculation if the free nucleon GT operator is quenched by $\sim$40% in nuclei. This quenching is usually attributed to a combination of $2\hbar\omega$ configuration mixing [15] and delta-hole states [16] shifting GT strength from lower to higher (and therefore unobserved) excitation energies. However, a more stringent test of the model is the calculation of GT strength distributions in the (n,p) reaction on $N>Z$ nuclei, where Pauli blocking and $0\hbar\omega$ mixing will have their largest effect. At present there are no published data for such distributions in the $1s$-$0d$ nuclei with $N>Z$.

The proportionality of the $(p,n)/(n,p)$ reaction and GT β^-/β^+ decay is characterized by the unit cross section $\hat{\sigma}$, the ratio of the $(p,n)/(n,p)$ cross section at zero energy and momentum transfer, $\sigma(q\rightarrow 0,\ \omega\rightarrow 0)$, and the corresponding GT transition probability B_{GT}. Exact proportionality of the $(p,n)/(n,p)$ and β^-/β^+-decay processes would yield a constant value of $\hat{\sigma}$ while distortions of the incoming and outgoing nucleon waves are expected to introduce a smooth dependence of $\hat{\sigma}$ on energy and target. However, although $\hat{\sigma}$ data for even-A targets do show a reasonably smooth A dependence, some other $\hat{\sigma}$ data do not [17]. In the (p,n)

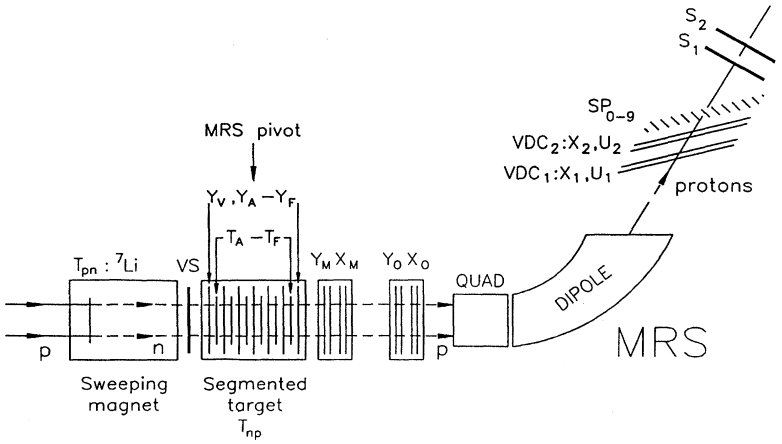

FIG. 1. Schematic of the TRIUMF (n,p) Charge Exchange Facility showing the primary (p,n) target, secondary (n,p) target, and Medium Resolution Spectrometer (MRS).

reaction it is found that the strong transitions to the isobaric analogs (IA's) of the target ground state for the odd-A targets ^{13}C, ^{15}N, and ^{39}K show values of $\hat{\sigma}$ that are as much as 50% greater than values for neighboring even-A targets [17]. This enhancement is not understood but there does not appear to be a comparable problem for transitions to non-IA's of the target ground state (g.s.) [2,18]. Although there is speculation that there may be a systematic difference between $\hat{\sigma}$ for even-A and odd-A targets [17], there is insufficient $\hat{\sigma}$ data for transitions to non-IA's of the target ground state for odd-A targets to be conclusive. This experiment, together with β-decay data and μ^- capture data, provide new data on $\hat{\sigma}$ for transitions to non-IA's of the target ground state on the odd-A target ^{23}Na.

In this paper we report measurements of the ^{23}Na(n,p) charge exchange reaction at an incident energy of 198 MeV and eight angles from 0° to 24°. From these data we determine the values of $B_{\rm GT}^{+}$ to low-lying levels in ^{23}Ne and the GT$^+$ strength distribution up to 25 MeV in excitation energy. These results are compared to complete and restricted 1s-0d shell model calculations and the role of $0\hbar\omega$ mixing and Pauli blocking is examined. Also compared are GT transition probabilites to low-lying states in ^{23}Ne extracted from the (n,p) data and μ^- capture data. Finally, utilizing both β-decay data and μ^- capture data, we extract unit cross sections from the ^{23}Na(n,p) data and make a comparison to the $\hat{\sigma}$ data compiled by Taddeucci *et al.* [17].

II. EXPERIMENTAL PROCEDURE

The experiment was performed at the TRIUMF cyclotron using beam line 4B and the Charge Exchange Facility. A schematic of the experimental setup is shown in Fig. 1. The primary proton beam, at 200 MeV and 400 nA, was directed onto a 110 mg/cm^2 thick ^{7}Li target producing, via the ^{7}Li(p,n) reaction to the ^{7}Be ground state and 427 keV excited state, a nearly monoenergetic neutron beam of 198 MeV. In addition the neutron spectrum shows a weak continuum due to many-body final states in the reaction with an intensity of about 1% compared to the peak. Downstream of the ^{7}Li target a sweeping magnet deflected the proton beam towards the beam dump while the undeflected neutron beam emerged from the sweeping magnet into the secondary target located 93 cm downstream of the primary target. A veto scintillator between the sweeping magnet and secondary target identified scattered protons. The arrangement yielded a neutron flux at the secondary target of about 1×10^5 s^{-1} cm^{-2}.

The secondary target consisted of six target planes (A–F) separated by seven-wire chamber planes (Y_V and Y_A–Y_F). The target segmentation enabled the correction of proton energy loss in the secondary target and, by employing one CH_2 target plane, normalization of the data via the known ^{1}H(n,p) differential cross section. A target stack consisted of six targets of area 2.3×4.6 cm^2 and separation 1.25 cm. A target wheel allowed three target stacks to be installed and switched in and out of the neutron beam remotely. The pattern of hits in the wire chambers Y_A–Y_F identified the struck target plane while the use of 6.0 μm Mylar windows and a 50% argon-50% CO_2 gas mixture minimized the ^{1}H(n,p) background. More details of the segmented target can be found in Ref. [19].

The Na targets were constructed by rolling Na metal to a thickness of about 100 mg/cm^2 and mounting slices of area 2.3×4.6 cm^2 between 6.0 μm Mylar windows in Cu support frames. The target stack for the ^{23}Na measurement was comprised of four Na targets, one CH_2 target (for normalization), and one Mylar target (for background subtraction). Two other target stacks, one containing six CH_2 targets and one containing five empty targets and one CH_2 target, were also mounted in the target wheel.

Protons emerging from the secondary target were momentum analyzed in the Medium Resolution Spectrometer (MRS). The magnetic elements of the MRS are a quadrupole magnet followed by a dipole magnet. A pair of front-end wire chambers (FEC0 and FECM) and a pair of drift chambers (VDC1 and VDC2) determine the particle trajectories at the entrance and focal plane of the spectrometer, respectively. Immediately downstream of the focal plane an array of paddle scintillators (SP_0–SP_9) and a pair of plastic scintillators (S1 and S2) provide time of flight and energy loss information. A valid event was defined as a delayed coincidence between the S1/S2 scintillators and the FEC0/FECM chambers, a valid hit pattern in the secondary target wire chambers, and no hit in the veto scintillator. More details of the MRS can be found in Ref. [20].

The overall energy resolution of the setup, due to the en-

TABLE I. Summary of ^{23}Na(n,p) data sets. Also listed are the ^{1}H(n,p) laboratory cross sections, σ_{np}(lab), used to normalize the ^{23}Na(n,p) data.

MRS angle	Mean scattering angle (cm)	σ_{np}(lab) (mb/sr)	MRS angle	Mean scattering angle (cm)	σ_{np}(lab) mb/sr
0°	1.5°	51.7	12°	13.9°	24.6
6°	5.6°	40.6	18°	18.1°	20.5
6°	7.7°	34.9	18°	20.3°	18.4
12°	11.8°	27.1	24°	24.1°	15.1

ergy spread in the neutron beam, energy loss in the secondary target, and energy resolution of the MRS, was 0.9 MeV. The solid angle subtended by the MRS was 3 msr and the angular acceptance of the MRS $\pm 2°$. ^{23}Na(n,p) data were collected at MRS angles of 0°, 6°, 12°, 18°, and 24°. In addition, at each angle data were collected with the CH_2 target stack and the empty target stack for acceptance, calibration, and background studies.

III. DATA REDUCTION

Off line a number of cuts was applied to the raw data. First, to remove backgrounds due the proton beam dump, a time of flight cut was applied between the FEC0/FECM chambers and the S1/S2 scintillators. Second, to remove backgrounds due to charged particles other than protons, an energy loss cut was applied to the S1/S2 scintillators. Third, to remove backgrounds due to the Cu target frames, trajectories determined by FEC0/FECM were traced to the secondary target and cuts applied to the track origin.

In addition, a cut was applied on the (n,p) scattering angle, dividing the data into pairs of data sets centered at 5.6°, 7.7°, 11.8°, 13.9°, 18.1°, 20.3°, and 24.1° each covering an angular range of $\pm 1°$. This cut was not applied to the 0° data set which, since the MRS was centered on 0°, already covered an angular range of $\pm 1°$. The mean (n,p) scattering angles corresponding to these $\pm 1°$ data sets are listed in Table I.

The 1.5° (n,p) spectra obtained from the ^{23}Na, CH_2, and Mylar targets, after application of these cuts, are shown in Fig. 2. The large peak at channel ~40 in each of the spectra is due to ^{1}H(n,p) charge exchange. In the ^{23}Na data this peak was due to the Mylar target windows and, to a lesser extent, NaOH contamination on the surface of the Na metal. As the scattering angle is increased the ^{1}H(n,p) peak moves through the ^{23}Na spectra. The smaller peak at channel ~140 is due to the ^{12}C(n,p)^{12}B$_{g.s.}$ charge exchange. In the ^{23}Na spectrum this peak was due to the Mylar target windows and, to a lesser extent, the CO_2 chamber gas.

Two different procedures were used to subtract the ^{1}H and ^{12}C backgrounds from the ^{23}Na data. In the first approach the Mylar spectra, normalized via the ^{1}H peak, were subtracted from the corresponding ^{23}Na spectra. However, since the Mylar windows were not the only source of the ^{1}H(n,p) and ^{12}C(n,p) backgrounds, the ^{1}H/^{12}C ratio in the Mylar data is not exactly the same as the ^{1}H/^{12}C ratio in the ^{23}Na data. Consequently this first approach oversubtracts the ^{12}C background. To correct this, in the second approach the Mylar and CH_2 spectra were first added in proportions that reproduce the ^{1}H/^{12}C ratio in the ^{23}Na data, and then these composite Mylar-CH_2 spectra, normalized via the ^{1}H peak, subtracted from the corresponding ^{23}Na spectra. The determination of the ^{1}H/^{12}C ratio in the ^{23}Na data was made by assuming that the ^{23}Na data underneath the ^{12}C(n,p)^{12}B$_{g.s.}$ peak varies smoothly from channel ~120 to channel ~150 in Fig. 2. In the subsequent analysis, however, no significant differences (compared to the statistical uncertainties) were found in the GT^{+} strength determined by the two different approaches.

After background subtraction the spectra were then normalized using the CH_2 target in the ^{23}Na target stack. The ^{1}H(n,p) differential cross sections were taken from the phase shift analysis computer code SAID [21] and are listed in Table I. The ^{23}Na(n,p) cross sections were then corrected

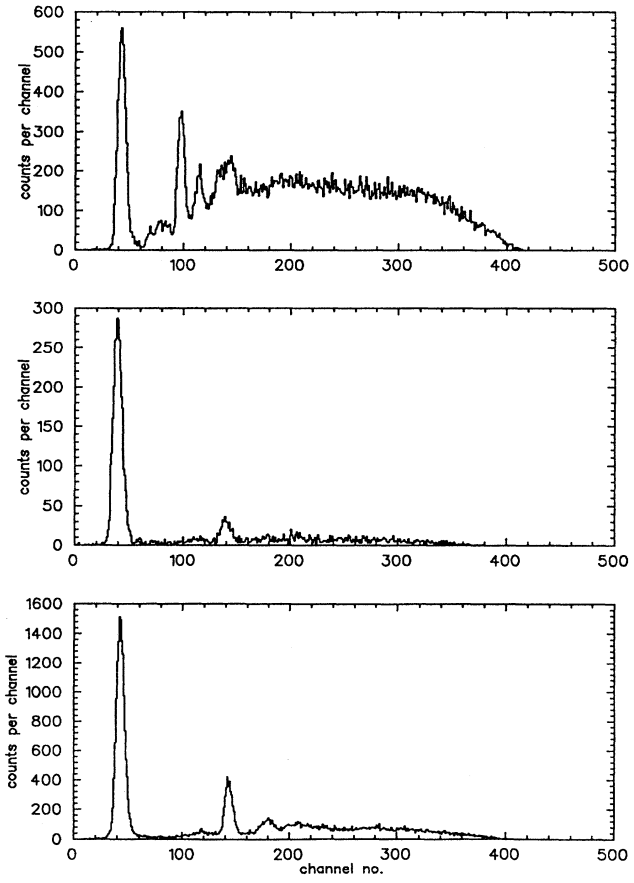

FIG. 2. The raw 1.5° (n,p) spectra from ^{23}Na (top), CH_2 (center), and Mylar (bottom).

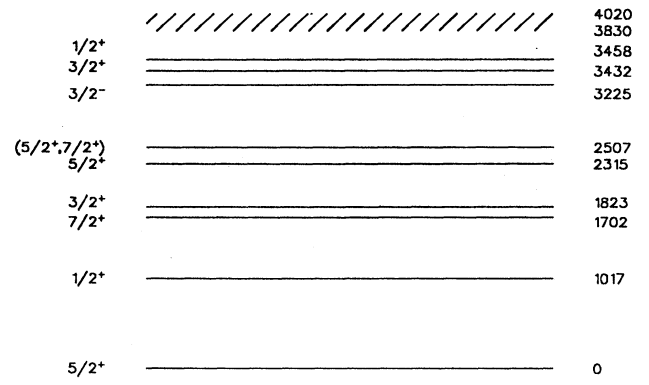

FIG. 3. Energy level diagram for low-lying states in ^{23}Ne. The excitation energies are in keV. The hatched region represents a cluster of states between 3830 and 4020 keV.

for the change in neutron flux and MRS acceptance between target F (the location of the CH_2 target) and targets B–E (the location of the ^{23}Na targets), and the variation of the MRS acceptance across the focal plane. These corrections were typically a few percent. Finally, the effects of the small tail in the neutron beam were corrected by a deconvolution procedure (this has been described in Ref. [4]).

IV. VALUES OF B^+_{GT} TO DISCRETE STATES IN ^{23}Ne

Figure 3 shows the energy level diagram for ^{23}Ne [22] and indicates six possible GT transitions below ~3.9 MeV to $1/2^+$, $3/2^+$, and $5/2^+$ states at excitation energies of 0, 1017, 1823, 2315, 3432, and 3458 keV. Figure 4 shows the 1.5° ^{23}Na(n,p) spectrum and indicates peaks at excitation energies corresponding to the 0, 1017, 1823, and 3432–3458 keV levels. The angular distributions of these peaks are all forward peaked (see, for example, Fig. 5), indicating their GT character, although the 0.9 MeV instrumental resolution means the 1823 keV GT transition may be contaminated by the 1702 keV non-GT transition and the 3432–3458 keV GT transitions may be contaminated by the 3225 keV non-GT transition.

To determine the cross sections of these GT transitions the ^{23}Na(n,p) spectra were fit with a sum of six Gaussian peaks. A Gaussian was included for each of the GT transitions to the 0, 1017, 1823, and 2315 keV states and one Gaussian for

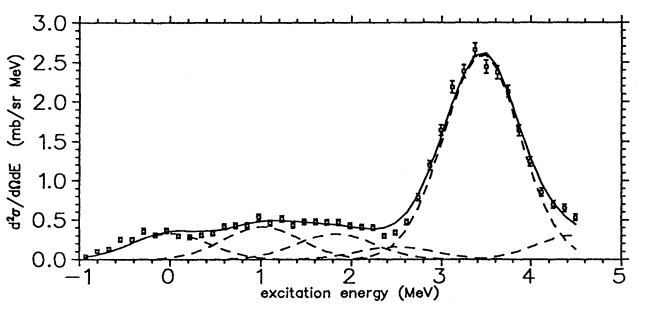

FIG. 4. Fit to the region -1.0 MeV $< E < +4.5$ MeV in the 1.5° ^{23}Na(n,p) spectrum.

the pair of GT transitions to the 3432–3458 keV states. Inclusion of the unobserved 2315 keV GT transition in the fit enabled an upper limit to be placed on its cross section. A sixth Gaussian was used to represent the background due to the cluster of states at ~3.9 MeV. In the fits the positions and widths of the peaks corresponding to the 0, 1017, 1823, 2315, and 3432–3458 keV levels were fixed at their known values while their amplitudes, and the amplitude, centroid, and width of the background peak, were varied. The result of the fit to the 1.5° ^{23}Na(n,p) data is shown in Fig. 4.

To determine the cross sections for the GT transitions to the 1823 and 3432–3458 keV states the contribution of the unresolved non-GT 1702 and 3225 keV transitions must be subtracted. In order to determine this non-GT contamination the angular distributions of the GT and non-GT transitions were calculated and fit to the cross section data. In the fits the shapes of the angular distributions were fixed while the amplitudes of the angular distributions were varied. To calculate the shapes of angular distributions we used shell model one-body transition densities (OBTD's) and the distorted wave impulse approximation (DWIA). For the positive parity 1702, 1823, 3432, and 3458 keV states we used the computer code OXBASH [23], the full $1s$-$0d$ model space, and the universal sd interaction, to determine the OBTD's. For the negative parity 3225 keV state we assumed a simple $0p_{3/2} \rightarrow 0d_{5/2}$ transition. For the DWIA calculation we used the computer code DW83 [24] and the effective nucleon-nucleon (NN) interaction of Franey and Love [25]. We generated the required optical potentials by convoluting the Franey-Love NN interaction [25] with a two-parameter matter distribution [26] using the computer code MAINX8 [27].

The calculated angular distributions for the 3225, 3432, and 3458 keV levels, and the resulting fit to the cross section data, are plotted in Fig. 5. The procedure yielded a negligible (~3%) contamination by the 3225 keV non-GT transition of the 3432–3458 keV GT transitions at 1.5°. A similar procedure yielded a negligible (~2%) contamination by the 1702 keV non-GT transition of the 1823 keV GT transition at 1.5°. The 1.5° cross sections for GT transition to the 0, 1017, 1823, 2315, and 3432–3458 keV states, after subtraction of the non-GT contamination, are listed in Table II.

To convert the 1.5° (n,p) cross sections to values of B^+_{GT} we used the standard equation [17]

$$B^+_{GT} = \sigma(1.5°)/\hat{\sigma} f(q,\omega), \tag{1}$$

where $\hat{\sigma}$ is the unit cross section appropriate to ^{23}Na and the factor $f(q,\omega)$ corrects $\sigma(1.5°)$ to zero energy (ω) and momentum (q) transfer. The factor $f(q,\omega)$ was calculated using the computer code DW83 and, since its value is almost independent of the DW83 input parameters, is known to high accuracy. Determination of the value of $\hat{\sigma}$ for ^{23}Na was, however, more problematic. Because of a possible systematic difference between values of $\hat{\sigma}$ for even-A and odd-A targets, a value of $\hat{\sigma}$ for ^{23}Na was estimated by extrapolation from the measured value for ^{13}C(n,p) [2]. Using an A dependence of $e^{-0.44A^{1/3}}$ as suggested by Taddeucci *et al.* [17] a value of $\hat{\sigma} = 8.9 \pm 0.45$ mb/sr was obtained.

Using $\hat{\sigma} = 8.9 \pm 0.45$ mb/sr and Eq. (1) we then obtained the values of B^+_{GT} for transitions to the 0, 1017, 1823, 2315, and 3432–3458 keV states listed in Table II. The entry for

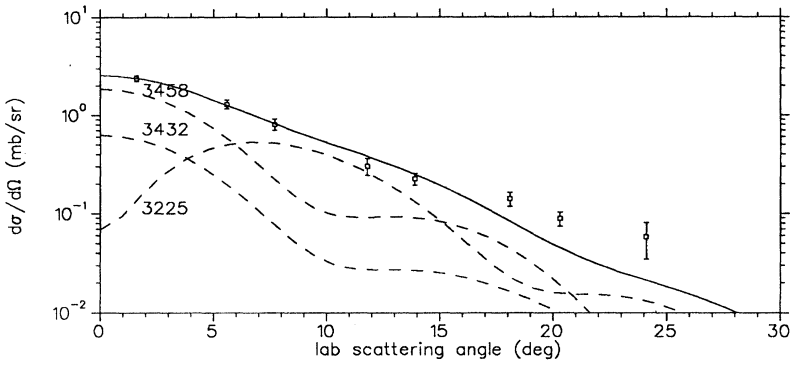

FIG. 5. Measured angular distribution of the 3432–3458 keV peak. The dashed lines are calculated angular distributions for transitions to the states at 3225, 3432, and 3458 keV and the solid curve their fit to the data.

the 3432 and 3458 keV states is the sum of their values of B^+_{GT} and the entry for the 2315 keV state is a upper limit on B^+_{GT}.

V. GT$^+$ STRENGTH VERSUS EXCITATION ENERGY

Figure 7, below, shows the (n,p) cross sections at each angle from 0° to 24° as a function of excitation energy (binned into channels 1.0 MeV wide). A multipole analysis of the data in each 1 MeV bin was carried out in order to determine the distribution of GT strength. The philosophy of the multipole decomposition is that these differential cross sections can be represented by an incoherent sum of theoretical angular distributions of definite angular momentum and parity transfer J^π according to the equation

$$\sigma^{\text{expt}}(\theta)=\sum_{J^\pi} C_{J^\pi}\sigma^{\text{th}}_{J^\pi}(\theta), \tag{2}$$

where $\sigma^{\text{expt}}(\theta)$ is the measured (n,p) differential cross section, $\sigma^{\text{th}}_{J^\pi}(\theta)$ is the theoretical angular distribution of angular momentum and parity transfer J^π, and C_{J^π} is the numerical coefficient that determines the amplitudes of each theoretical angular distributions. The values of C_{J^π} are obtained from a least squares fit of the sum of the theoretical angular distributions to the measured differential cross section. A detailed account of the multipole decomposition procedure can be found in Ref. [28].

The theoretical angular distributions were calculated using the DWIA computer code DW83 [24] and the effective NN interaction of Franey and Love [25]. They were calculated at 5.0 MeV intervals in excitation energy and interpolated to other excitation energies. For the required optical potentials we convoluted the Franey-Love NN interaction with a two-parameter matter distribution [26]. For the required one-body transition densities we used single-particle (SP) transitions.

To study the sensitivity of the results of the multipole decomposition to the choice of the SP transitions we explored a variety of plausible transitions. For example, in the case of the $J^\pi = 1^+$ multipole we tried the $0d_{5/2} \rightarrow 0d_{3/2}$, $0d_{5/2} \rightarrow 0d_{5/2}$ and $1s_{1/2} \rightarrow 1s_{1/2}$ transitions, and in the case of the $J^\pi = 1^-$ multipole we tried the $0p_{3/2} \rightarrow 0d_{5/2}$, $0p_{3/2} \rightarrow 0d_{3/2}$ and $0d_{5/2} \rightarrow 1f_{7/2}$ transitions. The angular distributions for these SP transitions are plotted in Fig. 6. It shows the similarity of the various 1^+ multipole shapes and various 1^- multipole shapes and, therefore, the choice of the SP transitions for the 1^+ and 1^- multipoles had little effect on the extracted GT$^+$ strength. Similar studies yielded similar conclusions for the 0^-, 2^+, and 3^- multipoles.

We also investigated the sensitivity of the multipole decomposition to the optical potentials by varying the radius r and diffuseness a in the two-parameter matter distribution used to calculate the potentials. The angular distributions obtained for different values of r and a are plotted in Fig. 6 and show the similarity of the various 1^+ multipole shapes and 1^- multipole shapes. Indeed, the differences in the shapes for various optical potentials are even smaller than the differences in the shapes for various SP transitions and, therefore, it was concluded they have a negligible effect on the extracted GT$^+$ strength.

To determine the necessary components for the multipole decomposition we tried a variety of sets of multipoles. It was found that the $J^\pi = 1^+$, 1^-, and 3^- multipoles were essential in the fit, the $J^\pi = 0^-$ and 2^+ multipoles were helpful in the fit, and other multipoles were unnecessary in the fit. The results of the multipole decomposition using the set of multipoles $J^\pi = 1^+$, 0^-, 1^-, 2^+, and 3^- and the SP transitions

TABLE II. 1.5° (n,p) cross sections, $\sigma(1.5°)$ and GT transition probabilities B^+_{GT} for transitions to low-lying discrete states in ^{23}Ne. A unit cross section of $\hat{\sigma} = 8.9 \pm 0.45$ mb/sr was used to determine the values of B^+_{GT}. Also tabulated are the B^+_{GT}'s calculated with the $1s$-$0d$ shell model.

J^π	E (keV)	$\sigma(1.5°)$ mb/sr	$f(q,\omega)$	B^+_{GT} (expt.)	B^+_{GT} (theory)
$5/2^+$	0	0.300 ± 0.051	0.89	0.038 ± 0.006	0.026
$1/2^+$	1017	0.364 ± 0.055	0.86	0.048 ± 0.007	0.111
$3/2^+$	1823	0.312 ± 0.058	0.86	0.041 ± 0.008	0.130
$5/2^+$	2315	≤ 0.162	0.85	≤ 0.021	0.040
$3/2^+$–$1/2^+$	3432–3458	2.35 ± 0.24	0.83	0.318 ± 0.033	0.335

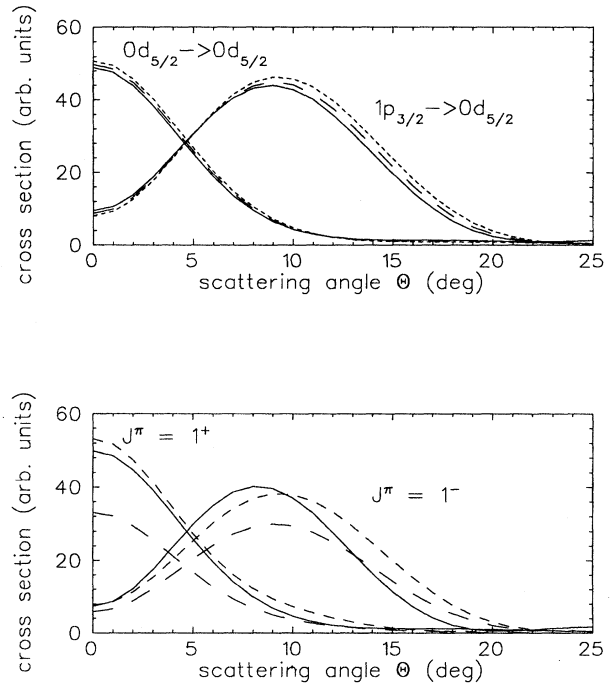

FIG. 6. Sensitivity of DWIA angular distributions to the choice of single-particle transitions (bottom) and the optical model parameters (top) for the 1^+ and 1^- multipoles. In the upper plot the solid curve corresponds to $r=2.6$ fm and $a=0.50$ fm, the long dashed curve to $r=2.8$ fm and $a=0.55$ fm, and the short dashed curve to $r=3.0$ fm and $a=0.60$ fm, where r and a are the radius and diffuseness parameters in the two-parameter matter distribution [26]. In the lower plot the solid, long dashed, and short dashed curves correspond to the single-particle transitions $0d_{5/2} \rightarrow 0d_{5/2}$, $1s_{1/2} \rightarrow 1s_{1/2}$ and $0d_{5/2} \rightarrow 0d_{3/2}$ for $J^\pi = 1^+$ and $0d_{5/2} \rightarrow 0f_{7/2}$, $0p_{3/2} \rightarrow 0d_{3/2}$ and $0p_{3/2} \rightarrow 0d_{5/2}$ for $J^\pi = 1^-$.

listed in Table III are shown in Fig. 7. The large peak centered at $\sim$3.5 MeV and $\sim 0°$ is identified as being of a Gamow-Teller nature and the large peak centered at $\sim$12 MeV and $\sim 9°$ is identified as being of a spin-dipole nature.

Using the distribution of the 1^+ cross section in Fig. 7, a unit cross section of 8.9 $\pm$ 0.45 mb/sr, and the $f(q,\omega)$ factors calculated with DW83, we obtained the GT$^+$ strength from 0 to 25 MeV excitation energy. The procedure gave a GT$^+$ strength from 0 to 10 MeV of $\Sigma B^+_{\rm GT} = 1.15 \pm 0.12$ and a GT$^+$ strength from 10 to 25 MeV of $\Sigma B^+_{\rm GT} = 1.63 \pm 0.17$ (in units where free neutron β decay yields $B^-_{\rm GT} = 3$). The uncertainties include both statistical errors in the multipole decomposition and an overall normalization error of 10%. The GT$^+$ strength from 0 to 10 MeV was found to be almost independent of the choice of multipoles and SP transitions. Eliminating the 0^- multipole from the decomposition, for example, yielded $\Sigma B^+_{\rm GT} = 1.19 \pm 0.13$ from 0 to 10 MeV. The GT$^+$ strength from 10 to 25 MeV, however, was found to be quite sensitive to details of the shape of DWIA angular distributions for other multipoles, particularly that for $\Delta L = 1$ transitions. This is because the angular distribution above 10 MeV is no longer forward peaked, making the GT$^+$ strength sensitive to the role of the other multipoles and hence the choice of multipoles and SP transitions. A similar sensitivity has been noted previously in Ref. [5].

TABLE III. The particle-hole configurations used in the multipole decomposition of the ^{23}Na(n,p) data.

J^π	p(h)$^{-1}$	J^π	p(h)$^{-1}$
0^-	$0d_{3/2}(0p_{3/2})^{-1}$	1^+	$0d_{5/2}(0d_{5/2})^{-1}$
1^-	$0d_{5/2}(0p_{3/2})^{-1}$	2^+	$0d_{5/2}(0s_{1/2})^{-1}$
3^-	$0d_{5/2}(0p_{3/2})^{-1}$		

VI. COMPARISON TO THE SHELL MODEL

Table II lists the measured and calculated values of $B^+_{\rm GT}$ for the GT transitions to discrete states in ^{23}Ne. The calculations were performed using the shell model computer code OXBASH [23], the complete $1s$-$0d$ model space, the universal sd interaction, and the free nucleon GT operator with $g_a = 1.251$. The table reveals a similar pattern in the experimental and theoretical $B^+_{\rm GT}$ distribution for the discrete states; both indicate a weak transition to the 2315 keV state, intermediate strength transitions to the 1017 and 1823 keV states, and a strong transition to the 3432–3458 keV doublet. However, the experimental values of $B^+_{\rm GT}$ are generally (with the exception of the g.s.-g.s. transition) smaller than the theoretical values of $B^+_{\rm GT}$. The ratio between the measured and calculated sum of the values of $B^+_{\rm GT}$ to discrete states is 0.74 $\pm$ 0.09.

Figure 8 and Table IV show the measured and calculated GT$^+$ strength versus excitation energy. The calculated GT$^+$ strength has been smeared using a Gaussian of 0.9 MeV full width at half maximum (FWHM) to represent the instrumental resolution. Again, the calculations were performed using the complete $1s$-$0d$ model space, the universal sd interaction, and the free nucleon GT operator with $g_a = 1.251$. The main features of the calculated GT$^+$ strength are a peak at $\sim$3.5 MeV, a broad plateau from 0 to 10 MeV, and little strength above 10 MeV. This is similar to the measured GT$^+$ strength which also shows a peak at $\sim$3.5 MeV, a broad plateau from 0 to 10 MeV, and less strength above 10 MeV. However, the sums of GT$^+$ strength between 0 and 10 MeV MeV are 1.15 $\pm$ 0.12 units (experiment) and 1.56 units (theory), yielding a ratio of 0.74 $\pm$ 0.08, consistent with the sum of $B^+_{\rm GT}$ to ^{23}Ne discrete states. Also, although both the experimental and theoretical GT$^+$ distributions decrease above 10 MeV, the experimental strength is much larger than the theoretical strength. This is consistent with the removal of GT$^+$ strength from lower to higher excitation energies.

Finally, what is the role of $0\hbar\omega$ configuration mixing in determining the GT$^+$ strength in ^{23}Na? Figure 9 shows a running sum of the GT$^+$ strength versus excitation energy for the data, the full shell model calculation, and a restricted shell model calculation. The restricted calculation employed a $(0d_{5/2})^7$ configuration for the $3/2^+$ g.s. of ^{23}Na and a $(0d_{5/2})^6(0d_{3/2})^1$ configuration for the $1/2^+$, $3/2^+$, and $5/2^+$ states in ^{23}Ne. The results reveal a factor of 0.32 reduction in $\Sigma B^+_{\rm GT}$ between the full and restricted shell model calculations and indicate the importance of $0\hbar\omega$ mixing and Pauli blocking in governing the GT$^+$ strength on ^{23}Na. The results

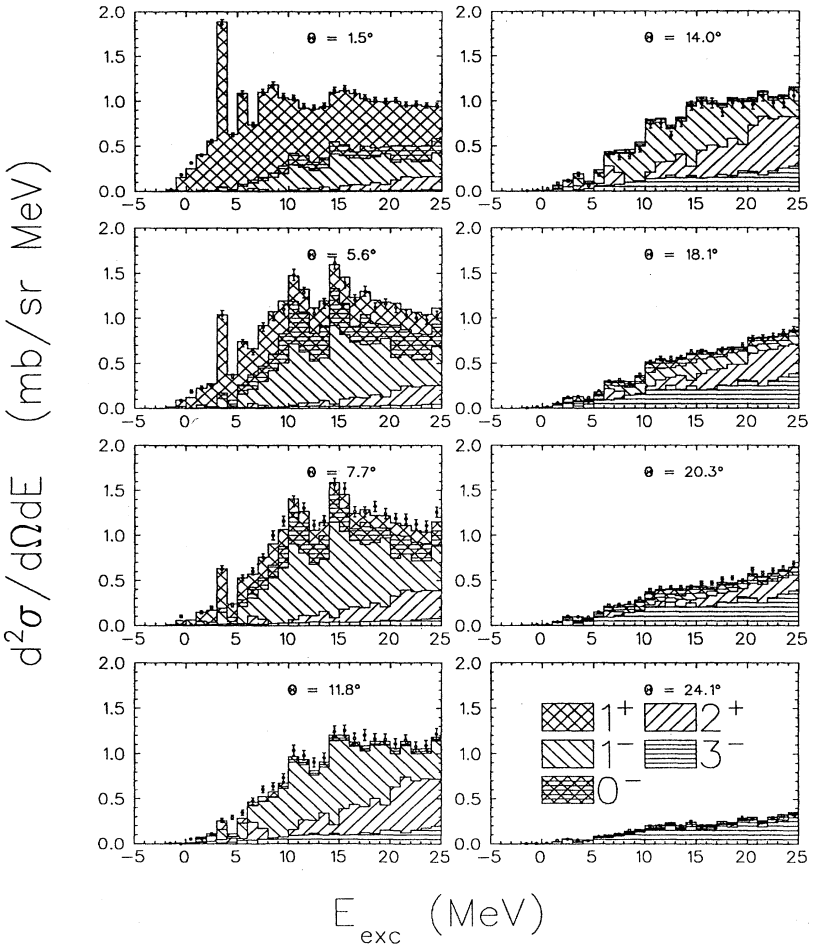

FIG. 7. The results of the multipole decomposition for ^{23}Na(n,p).

are consistent with the calculations of Auerbach *et al.* [29]. They found large decreases in GT$^+$ strength in the $N>Z$ nuclei ^{26}Mg, ^{54}Fe, and ^{56}Ni due to $0\hbar\omega$ mixing, although an additional 40% global quenching of GT strength was still needed to reproduce the ^{26}Mg, ^{54}Fe, and ^{56}Ni data. This appears to be the case in ^{23}Na also.

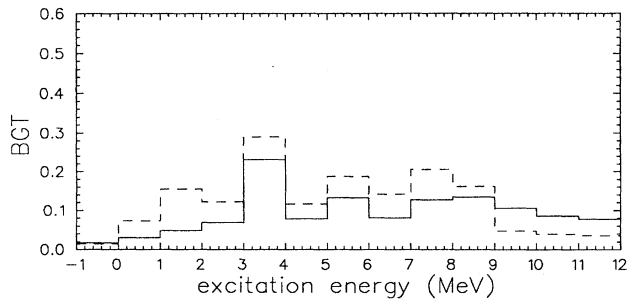

FIG. 8. Comparison of the measured (solid curve) and calculated (dashed curve) $B^+_{\rm GT}$ strength up to 12 MeV excitation energy. The calculation employed the complete $1s$-$0d$ model space, the universal sd interaction, and the free nucleon GT operator with $g_a = 1.251$. The units correspond to $B_{\rm GT} = 3$ for neutron β decay.

VII. COMPARISON TO THE (μ^-,ν) DATA

Figure 10 shows a comparison of the 1.5° (n,p) cross section data and (μ^-,ν) capture rate data to low-lying states in ^{23}Ne (the transition to the ^{23}Ne g.s. is not measured in the μ^- capture experiment). The similarity reflects the dominance of GT excitations in both the (n,p) and (μ^-,ν) data. In this section we quantify the comparison of the (n,p) and (μ^-,ν) data by comparing the values of $B^+_{\rm GT}$ obtained from the two processes.

In Ref. [30] values of $B^+_{\rm GT}$ for transitions to the 1017, 1823, 3432, and 3458 keV states are extracted, via two different approaches, from $\mu^-{}^{23}$Na capture rates. In the first approach all matrix elements except the GT matrix element are neglected in order to determine $B^+_{\rm GT}$. In the second approach matrix elements neglected in the first approach are calculated using the $1s$–$0d$ shell model in order to determine $B^+_{\rm GT}$. The resulting values of $B^+_{\rm GT}$, obtained in Ref. [30] via these two approaches, are reproduced in Table V.

Table V shows the values of $B^+_{\rm GT}$ for the 1017, 3432, and 3458 keV transitions, obtained via the two different approaches, differ by only 10%, 11%, and 16%, respectively. These small differences are due to the dominance of the GT matrix element in these μ^- capture transitions. Table V, however, also shows that the values of $B^+_{\rm GT}$ for the 1823 keV

TABLE IV. 1.5° (n,p) cross sections, the factors $f(q,\omega)$, and GT$^+$ strength as a function of excitation energy. The value $\hat{\sigma}$ = 8.9 ± 0.45 mb/sr was used to determine the GT$^+$ strength.

E_x (MeV)	$\sigma_{GT}(1.5°)$ (mb/sr)	$f(q,\omega)$	B^+_{GT}
−0.50	0.145	0.908	0.017
0.50	0.252	0.889	0.032
1.50	0.395	0.870	0.050
2.50	0.549	0.850	0.072
3.50	1.834	0.831	0.248
4.50	0.607	0.812	0.084
5.50	1.013	0.793	0.143
6.50	0.612	0.774	0.089
7.50	0.946	0.755	0.141
8.50	0.976	0.736	0.149
9.50	0.757	0.718	0.119

transition, obtained via the two different approaches, differ by 66%. This large difference indicates that the GT matrix element is not dominant in this transition and that this estimate of B^+_{GT} is subject to a large uncertainty.

Table V also lists the values of B^+_{GT} for the 1017, 1823, and 3432–3458 keV transitions obtained from the ^{23}Na(n,p) data. It shows that the values of B^+_{GT} extracted from the (n,p) and (μ^-,ν) data are, within experimental uncertainties, consistent. For example, the sum of the values of B^+_{GT} to the 3432–3458 keV doublet from the (n,p) and (μ^-,ν) data are 0.313 ± 0.033 and 0.28 ± 0.05, respectively. The values of B^+_{GT} for the 1017 and 1823 keV transitions also agree although the comparison is limited by the large uncertainties in the μ^- capture rates.

The general consistency of the values of B^+_{GT} to low-lying states in ^{23}Ne obtained from the (n,p) data, μ^- capture data, and full 1s-0d shell model calculation build confidence in the value of the weak pseudoscalar coupling, g_p, extracted from a recent measurement of the hyperfine effect in μ^- capture on ^{23}Na [13].

VIII. UNIT CROSS SECTIONS

The ground state of ^{23}Ne undergoes β^- decay to the ground state of ^{23}Na and provides an independent determination of the GT transition probability for the transition ^{23}Na(3/2$^+$,0) → ^{23}Ne(5/2$^+$,0). A value for the unit cross section for this transition can therefore be determined using Eq. (1). Substituting into this equation $\sigma(1.5°)$ = 0.30 ± 0.05 mb/sr, B^+_{GT} = 0.0315 ± 0.0004 [31], and $f(q,\omega)$ = 0.89 we obtained $\hat{\sigma}$ = 10.7 ± 1.8 mb/sr.

In addition to determining $\hat{\sigma}$ using β-decay data it is interesting to explore determining $\hat{\sigma}$ using μ^- capture data. The advantage of using μ^- capture is that states inaccessible to β decay are accessible to μ^- capture, but a disadvantage is the large momentum transfer and, therefore, the contribution of matrix elements other than the GT matrix element. However, with the philosophy of simply exploring the use of μ^- capture to determine unit cross sections, we have used Eq. (1) and the μ^- capture values of B^+_{GT} in Table V to calculate unit cross sections for transitions to the 1017, 1823, and 3432–3458 keV states in ^{23}Ne. We obtained 7.0 ± 2.3, 11.3 ± 3.5, and 10.1 ± 2.5 mb/sr, respectively, yielding a weighted mean for the μ^--capture-determined unit cross sections of $\hat{\sigma}$ = 9.6 ± 1.6 mb/sr.

The values of $\hat{\sigma}$ obtained using the β-decay and μ^- capture data, 10.7 ± 1.8 and 9.6 ± 1.6 mb/sr, respectively, although somewhat larger than the value of 8.9 ± 0.45 mb/sr extrapolated from the ^{13}C(n,p) result, are consistent within their uncertainties. The β-decay and μ^- capture $\hat{\sigma}$ values are also larger than the general trend of the $\hat{\sigma}$ data for even-A

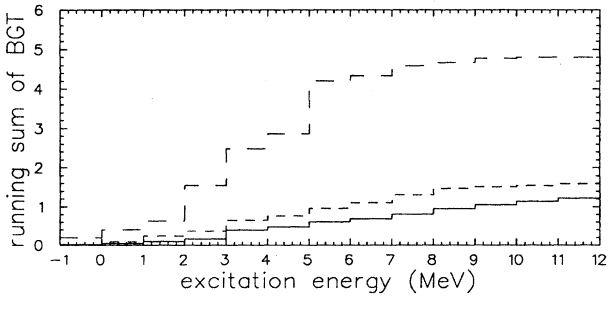

FIG. 9. The running sum of B^+_{GT} up to 12 MeV excitation energy. The long dashed line is the restricted 1s-0d shell model, the short dashed line is the complete 1s-0d shell model, and the solid line is the experimental data.

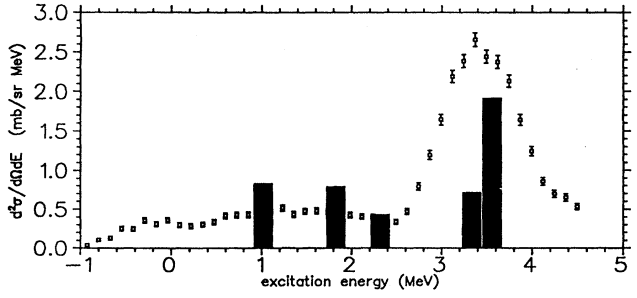

FIG. 10. Comparison of 1.5° ^{23}Na(n,p) cross section and μ^-^{23}Na capture rates. The overall normalization of the μ^- data is arbitary. The uncertainities in the μ^- capture rates are not shown.

TABLE V. Summary of GT transition probabilities B_{GT}^{+}'s obtained from μ^{-} ^{23}Na capture data. Column 3 lists B_{GT}^{+}'s obtained by neglecting non-GT matrix elements and column 4 lists the B_{GT}^{+}'s obtained by including non-GT contributions to the matrix elements. Also shown are the B_{GT}^{+}'s obtained from the (n,p) data and unit cross sections calculated using the μ^{-} capture data. The ^{23}Na g.s. to ^{23}Ne g.s. transition is not measured in the μ^{-} capture experiment.

J^{π}	E (keV)	B_{GT}^{+} (negl.)	B_{GT}^{+} (calc.)	B_{GT}^{+} (n,p)	$\hat{\sigma}$ (mb/sr)
$5/2^{+}$	0			0.038 ± 0.006	
$1/2^{+}$	1017	0.068 ± 0.019	0.061 ± 0.017	0.048 ± 0.007	7.0 ± 2.3
$3/2^{+}$	1823	0.094 ± 0.025	0.032 ± 0.008	0.041 ± 0.008	11.3 ± 3.5
$3/2^{+}$	3432	0.085 ± 0.018	0.094 ± 0.020		
$1/2^{+}$	3458	0.16 ± 0.04	0.19 ± 0.04		
$1/2^{+}$–$3/2^{+}$	3432–3458	0.24 ± 0.05	0.28 ± 0.05	0.318 ± 0.033	10.1 ± 2.5

targets compiled by Taddeucci *et al* [20]. This could be indicative of an even-A–odd-A effect in $\hat{\sigma}$, but concerns over the validity of the proportionality of the $(n,p)/(p,n)$ and β^{-}/β^{+} reactions for weak transitions [32] such as ^{23}Na$(3/2^{+},0) \rightarrow$ ^{23}Ne$(5/2^{+},0)$ (B_{GT}^{+} = 0.0315) and uncertainties about the determination of B_{GT}^{+} from μ^{-} capture data make it impossible to reach a more definite conclusion.

Last, using the DWIA, we have calculated unit cross sections for the ^{23}Na(n,p) transitions to the 0, 1017, 1823, and 3432–3458 keV states in ^{23}Ne. The calculations were performed, as previously described, using OBTD's obtained from a full $1s$-$0d$ shell calculation and optical potentials obtained by convoluting the Franey-Love NN interaction with a two-parameter matter distribution. The resulting values of $\hat{\sigma}$ are 9.44, 7.44, 7.48, and 7.63 mb/sr for the 0, 1017, 1823, and 3432–3458 keV states, respectively. They indicate that the value of $\hat{\sigma}$ for the weak g.s.-g.s. transition is 25% larger than the values of $\hat{\sigma}$ for the stronger 1017, 1823, and 3432–3458 keV transitions. This result is consistent with the measured values of $\hat{\sigma}$ which also indicate a larger value of $\hat{\sigma}$ for the g.s.-g.s. transition (10.7 ± 1.8 mb/sr) than the mean value of $\hat{\sigma}$ for the 1017, 1823, and 3432-3458 keV transitions (9.6 ± 1.6 mb/sr) although the uncertainties are too large for a definite conclusion. The results of these calculations, indicating a departure from proportionality of the (n,p) 0° cross section and B_{GT}^{+} for weak GT transitions, is in agreement with the recent work of Austin *et al.* [32].

IX. SUMMARY

In summary, we have measured the ^{23}Na(n,p) differential cross section at an incident energy of 198 MeV and eight angles from 0° to 24° and from these data determined GT transition probabilities to low-lying $1/2^{+}$, $3/2^{+}$, and $5/2^{+}$ ^{23}Ne levels and the GT^{+} strength distribution up to 25 MeV excitation energy.

We found the distribution of GT^{+} strength to discrete states and GT^{+} strength from 0 to 10 MeV to be in reasonable agreement with a full $1s$-$0d$ shell model calculation when normalized by a factor of about 0.74. In addition, we found an excess of measured GT^{+} strength compared to the calculated GT^{+} strength above 10 MeV, although uncertainties in the multipole decomposition make a quantitative statement about the excess GT^{+} strength problematic. These results for ^{23}Na are consistent with the observation of a 40% quenching of GT strength at low energies and the removal of GT strength to higher energies reported for $N=Z$ nuclei in the sd shell [14].

We have also examined unit cross sections determined from the ^{23}Na(n,p) measurement utilizing both β-decay and μ^{-} capture data. We obtained $\hat{\sigma}$ = 10.7 ± 1.8 mb/sr and $\hat{\sigma}$ = 9.6 ± 1.6 mb/sr from the β-decay and μ^{-} capture data, respectively, consistent with the value of 8.9 ± 0.45 mb/sr extrapolated from the ^{13}C(n,p) value. These measured unit cross sections are, however, larger than the trend of the even-A $\hat{\sigma}$ data although concerns about the weak β-decay transition and the use of μ^{-} capture transitions prevent any definitive conclusions. Calculations of these unit cross sections using the DWIA are consistent with the measured values of $\hat{\sigma}$ and suggest a departure from proportionality for the weak (B_{GT}^{+} = 0.0315) ^{23}Na g.s. to ^{23}Ne g.s. transition.

Last, we have compared the ^{23}Na(n,p) data with ^{23}Na(μ^{-},ν) data and found reasonable agreement between the values of B_{GT}^{+} to low-lying states in ^{23}Ne obtained from the two processes. The general consistency of the (n,p) and (μ^{-}, ν) data, and also the full $1s$-$0d$ shell model calculation, build confidence in the recent determination of the weak pseudoscalar coupling g_p from a measurement of the hyperfine effect in μ^{-} capture on ^{23}Na [13]. This experiment indicates a value of the weak pseudoscalar coupling that is consistent with the PCAC hypothesis but in disagreement with recent claims of a large renormalization of g_p in nuclei.

ACKNOWLEDGMENTS

We would like to thank Prof. Alex Brown for assistance with the shell model calculations, the TRIUMF technical staff for the smooth operation of the TRIUMF cyclotron, and the National Science Foundation (U.S.) and the Natural Sciences and Engineering Research Council (Canada) for their financial support.

[1] C.D. Goodman, C.A. Goulding, M.B. Greenfield, J. Rapaport, D.E. Bainum, C.C. Foster, W.G. Love, and F. Petrovich, Phys. Rev. Lett. **44**, 1755 (1980).

[2] K.P Jackson, A. Celler, W.P. Alford, R. Abegg, R.E. Azuma, C.K. Campbell, S. El-Kateb, D. Frekers, P.W. Green, O. Hausser, R.L. Helmer, R.S. Henderson, K.H. Hicks, R. Jeppesen, P. Lewis, C.A. Miller, A. Moalem, M.A. Moinester, R.B. Schubank, G.G. Shute, B.M. Spicer, M.C. Vetterli, A.I. Yavin, and S. Yen, Phys. Lett. **B** 201, 25 (1988).

[3] T. Ronnqvist, H. Conde, N. Olsson, E. Ramstrom, R. Zorro, J. Blomgren, A. Halansson, A. Ringbom, G. Tibell, O. Jonsson, L. Nilsson, P.-U. Renberg, S.Y. van der Werf, W. Unkelbach, and F.P. Brady, Nucl. Phys. **A563**, 225 (1993).

[4] M.C. Vetterli, O. Hausser, R. Abegg, W.P. Alford, A. Celler, D. Frekers, R. Helmer, R. Henderson, K.H. Hicks, K.P. Jackson, R.G. Jeppesen, C.A. Miller, K. Raywood, and S. Yen, Phys. Rev. C **40**, 559 (1989).

[5] S. El-Kateb, K.P. Jackson, W.P. Alford, R. Abegg, R.E. Azuma, B.A. Brown, A. Celler, D. Frekers, O. Hausser, R. Helmer, R.S. Henderson, K.H. Hicks, R. Jeppesen, J.D. King, K. Raywood, G.G. Shute, B.M. Spicer, A. Trudel, M. Vetterli, and S. Yen, Phys. Rev. C **49**, 3128 (1994).

[6] W.P. Alford, R.L. Helmer, R. Abegg, A. Celler, D. Frekers, P. Green, O. Hausser, R. Henderson, K.H. Hicks, K.P. Jackson, R. Jeppesen, C.A. Miller, A. Trudel, M. Vetterli, S. Yen, R. Pourang, J. Watson, B.A. Brown, and J. Engel, Nucl. Phys. **A531**, 97 (1991).

[7] J. Rapaport, T. Tadduecci, P. Welch, C. Gaarde, J. Larsen, C. Goodman, C.C. Foster, C.A. Goulding, D. Horen, E. Sugarbaker, and T. Masterson, Phys. Rev. Lett. **40**, 1518 (1981).

[8] M. Gell-Mann and M. Levy, Nuovo Cimento **16**, 705 (1960); Y. Nambu, Phys. Rev. Lett. **4**, 380 (1960).

[9] M.L. Goldberger and S.B. Treiman, Phys. Rev. **110**, 1178 (1958).

[10] G. Bardin, J. Duclos, A. Magnon, J. Martino, A. Richter, E. Zavattini, A. Bertin, M. Piccinini, A. Vitale, and D. Measday, Nucl. Phys. **A352**, 365 (1981), and references therein.

[11] A. Frischknecht, M. Dobeli, W. Stehling, G. Strassner, P. Troul, J.C. Alder, C. Joseph, J.F. Loude, J.P. Perroud, D. Rugger, M.T. Tran, and H. Panke, Phys. Rev. C **38**, 1996 (1988).

[12] D.S. Armstrong, S. Ahmad, R.A. Burnham, T.P. Gorringe, M.D. Hasinoff, A.J. Larabee, C.E. Waltham, G. Azeulos, J.A. Macdonald, J-M. Pouttisou, M. Blecher, D.H. Wright, E.T.H. Clifford, P. Depommier, R. Poutissou, H. Mes, and B.C. Robertson, Phys. Rev. C **40**, 1100 (1989); **43**, 1425 (1991); **46**, 1094 (1992).

[13] T.P. Gorringe, B. Johnson, D.S. Armstrong, J. Bauer, M.A. Kovash, M.D. Hasinoff, D.F. Measday, B.A. Moftah, R. Porter, and D.H. Wright, Phys. Rev. Lett. **72**, 3472 (1994).

[14] B.D. Anderson, N. Tamimi, A.R. Baldwin, M. Elaasar, R. Madey, D.M. Manley, M. Mostajabodda'vati, J.W. Watson, W.M. Zhang, and C.C. Foster, Phys. Rev. C **43**, 50 (1991).

[15] I.S. Towner and F.C. Khanna, Phys. Rev. Lett. **42**, 51 (1979); E. Oset and M. Rho, *ibid.* **42**, 47 (1979).

[16] M. Rho, Nucl. Phys. **A231**, 493 (1974).

[17] T.N. Taddeucci, C.A. Goulding, T.A. Carey, R.C. Byrd, C.D. Goodman, C. Gaarde, J. Larsen, D. Horen, J. Rapaport, and E. Sugarbaker, Nucl. Phys. **A469**, 125 (1987).

[18] J.L. Mildenberger, W.P. Alford, A. Celler, O. Hausser, K.P. Jackson, B. Larson, B. Pointon, A. Trudel, M.C. Vetterli, and S. Yen, Phys. Rev. C **43**, 1777 (1991).

[19] R.S. Henderson, W.P. Alford, D. Frekers, O. Hausser, R.L. Helmer, K.H. Hicks, K.P. Jackson, C.A. Miller, M.C. Vetterli, and S. Yen, Nucl. Instrum. Methods Phys. Res. Sect. A **257**, 97 (1987).

[20] MRS Manual Rev. 2.0, TRIUMF, 1988 (unpublished).

[21] R.A. Arndt and L.D. Soper, Computer code SAID (scattering analysis interactive dial-in) program (SM90) (unpublished); R.A. Arndt *et al.*, Phys. Rev. D **45**, 3995 (1992).

[22] P.M. Endt, Nucl. Phys. **A521**, 1 (1990).

[23] B.A. Brown, A. Etchegoyen, W.D.M. Rae, and N.S. Godwin, Computer code OXBASH (Oxford-Buenos-Aires-MSU shell model), MSUCL Report No. 524, 1986.

[24] R. Schaeffer and J. Raynal, Computer code DWBA70, J.R. Comfort, extended version DW83, Arizona State University, 1984 (unpublished).

[25] M.A. Franey and W.G. Love, Phys. Rev. C **31**, 488 (1985).

[26] H. de Vries, C.W. de Jager, and C. de Vries, At. Data Nucl. Data Tables **36**, 495 (1987).

[27] T. Cooper, computer code MAINX8, modified by R.G. Jeppesen (unpublished).

[28] M.A. Moinester, Can. J. Phys. **65**, 660 (1987).

[29] N. Auerbach, G.F. Bertsch, B.A. Brown, and L. Zhao, Nucl. Phys. **A556**, 190 (1993).

[30] B. Johnson, Ph.D. thesis, University of Kentucky, 1994; B. Johnson *et al.* (unpublished).

[31] B.A. Brown and B.H. Wildenthal, At. Data Nucl. Data Tables **33**, 347 (1985).

[32] S.M. Austin, N. Anantaraman, and W.G. Love, Phys. Rev. Lett. **73**, 30 (1994).